SANDIA REPORT
SAND99-0662
Unlimited Release
Printed November 1999

Z-Pinch Generated X-Rays in Static-Wall-Hohlraum Geometry Demonstrate Potential for Indirect-Drive ICF Studies

T. W. L. Sanford, R. E. Olson, R. C. Mock, G. A. Chandler, D. E. Hebron, R. J. Leeper, T. J. Nash, L. E. Ruggles, W. W. Simpson, K. W. Struve, R. A. Vesey, R. L. Bowers, W. Matuska, D. L. Peterson, and R. R. Peterson

Prepared by
Sandia National Laboratories
Albuquerque, New Mexico 87185 and Livermore, California 94550

Sandia is a multiprogram laboratory operated by Sandia Corporation, a Lockheed Martin Company, for the United States Department of Energy under Contract DE-AC04-94AL85000.

Sandia National Laboratories

Issued by Sandia National Laboratories, operated for the United States Department of Energy by Sandia Corporation.

Available to DOE and DOE contractors from
Office of Scientific and Technical Information
P.O. Box 62
Oak Ridge, TN 37831

Prices available from (703) 605-6000
Web site: http://www.ntis.gov/ordering.htm

Available to the public from
National Technical Information Service
U.S. Department of Commerce
5285 Port Royal Rd
Springfield, VA 22161

NTIS price codes
Printed copy: A03
Microfiche copy: A01

SAND99-0662
Unlimited Release
Printed November1999

Z-Pinch Generated X-Rays in Static-Wall-Hohlraum Geometry Demonstrate Potential for Indirect-Drive ICF Studies

T. W. L. Sanford*, R. E. Olson, R. C. Mock, G. A. Chandler, D. E. Hebron, R. J. Leeper, and T. J. Nash
Diagnostics and Target Physics

L. E. Ruggles, and W. W. Simpson
Z-Pinch Experiments and Advanced Diagnostics

K. W. Struve
Load Coupling and Z-Pinch Source Development

R. A. Vesey
Target and Z-Pinch Theory

Sandia National Laboratories
P. O. Box 5800
Albuquerque, New Mexico 87185

R. L. Bowers, W. Matuska, and D. L. Peterson
Los Alamos National Laboratory
Los Alamos, New Mexico 87545-0010

R. R. Peterson
University of Wisconsin
Madison, Wisconsin 53706

Abstract follows

*Paper MO1c6 presented at the First International Conference on Inertial Fusion Sciences and Applications (Bordeaux, France, September 12-17, 1999).

ABSTRACT

Hohlraums of full ignition scale (6-mm diameter by 7-mm length) have been heated by x-rays from a z-pinch target on Z to a variety of temperatures and pulse shapes which can be used to simulate the early phases of the National Ignition Facility (NIF) temperature drive. The pulse shape is varied by changing the on-axis target of the z pinch in a static-wall-hohlraum geometry [*Fusion Technol.* **35**, 260 (1999)]. A 2-μm-thick walled Cu cylindrical target of 8-mm diameter filled with 10 mg/cm^3 CH, for example, produces *foot-pulse* conditions of ~85 eV for a duration of ~10 ns, while a solid cylindrical target of 5-mm diameter and 14-mg/cm^3 CH generates *first-step-pulse* conditions of ~122 eV for a duration of a few ns. Alternatively, reducing the hohlraum size (to 4-mm diameter by 4-mm length) with the latter target has increased the peak temperature to ~150 eV, which is characteristic of a *second-step-pulse* temperature. In general, the temperature T of these x-ray driven hohlraums is in agreement with the Planckian relation $T \sim (P/A)^{1/4}$. P is the measured x-ray input power and A is the surface area of the hohlraum. Fully-integrated 2-D radiation-hydrodynamic simulations of the z pinch and subsequent hohlraum heating show plasma densities within the useful volume of the hohlraums to be on the order of air or less.

ACKNOWLEDGEMENTS

M. G. Haines (Imperial College) and M. K. Matzen are thanked for useful discussions; M. S. Derzon, S. Dropinski, T. L. Gilliland, R. E. Hawn, D. Jobe, J. S. McGurn, J. S. Seamen, W. A. Stygar, J. A. Torres, and the Z crew for their dedicated technical support; J. S. DeGroot (UCD) for his careful review of the paper; and T. L. Cutler for editing, and for reformatting the paper into the correct Sandia Report format.

CONTENTS

INTRODUCTION.....5

EXPERIMENTAL ARRANGEMENT.....7

HOHLRAUM TEMPERATURE PULSE SHAPES.....10

HOHLRAUM CHARATERISTICS.....10

CONCLUSIONS.....13

REFERENCES.....13

DISTRIBUTION.....15

FIGURES

1. Comparison of representative NIF radiation temperature profiles (W and D) with those measured for Shots Z251, Z441, and Z442. 5

2. Schematic of single-sided, static-wall-hohlraum geometry. 6

3. Measured hohlraum temperature as a function of the measured on-axis x-ray power without the hohlraum present, for the indicated shot pairs. Shown also is that expected from the $T\sim(P/A)^{1/4}$ Planckian relation, using a calculated normalization point at 13-TW [15]. 8

4. Peak power, risetime, and duration to final stagnation of measured on-axis x-ray pulse versus shell thickness, for a 8-mm diameter PST with 6 mg/cc foam fill. 9

5. Comparison of the simulated radiation temperature and lower bound on the wall temperature with that measured for Shot Z441. 11

6. Simulated on-axis plasma density 2-mm above the REH for Shot Z441. 12

INTRODUCTION

Radiation environments characteristic of those encountered during the low-temperature *foot pulse* and subsequent higher-temperature *early-step pulses (Figure1)* required for indirect-drive ICF ignition on NIF [1, 2] are desired in order to provide a platform to better understand the dynamics of NIF hohlraums and capsules prior to NIF completion [3]. In particular, (1) the dynamics of the proposed He-fill wall tamping and hole closure in the NIF hohlraum, and (2) improved capsule ablator burn-through rates and shock propagation velocities [4] are needed to better design these components. In this paper, we show that an axial hohlraum using the static-wall-hohlraum geometry [5] heated by x-rays from a z-pinch on the Z generator [6] is capable of providing environments for such pre-NIF studies.

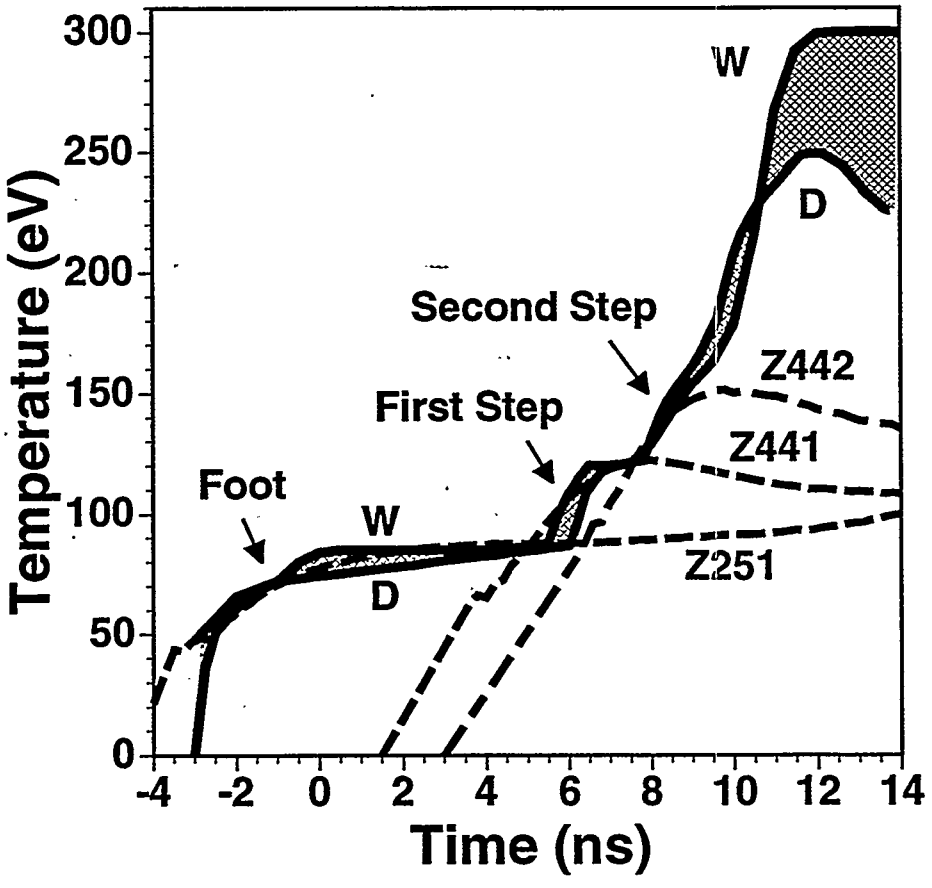

Figure 1. Comparison of representative NIF radiation temperature profiles (W [13] and D [14]) with those measured for Shots Z251, Z441, and Z442.

In this single-sided x-ray drive *(Figure 2)*, the axial hohlraum is placed above a pulse-shaping target (PST) within an x-ray-producing z-pinch. X-rays produced in the PST enter the axial hohlraum through a radiation-entrance-hole (REH) and heat its walls. The x-rays are generated in the PST by the thermalization of the kinetic energy acquired when a cylindrical plasma shell, created by one or more wire arrays, collides with the PST within the z-pinch. In this arrangement, the wires (which are made of W) form an annular plasma radiation case [7] by the time they strike the PST (first strike). The high-atomic-number radiation case traps a fraction of the x-rays produced in the PST (as in a dynamic-hohlraum [8]), and radiation flows from the interior of the PST into the axial hohlraum, whose walls remain relatively static. A low-opacity foam fill is used in the PST so that as final stagnation is approached, the foam remains transparent to the x-rays, yet provides a back-pressure on the imploding mass. The back-pressure enables additional energy to be extracted from the acceleration and increases the x-ray energy generated as the magnetic field compresses the PST.

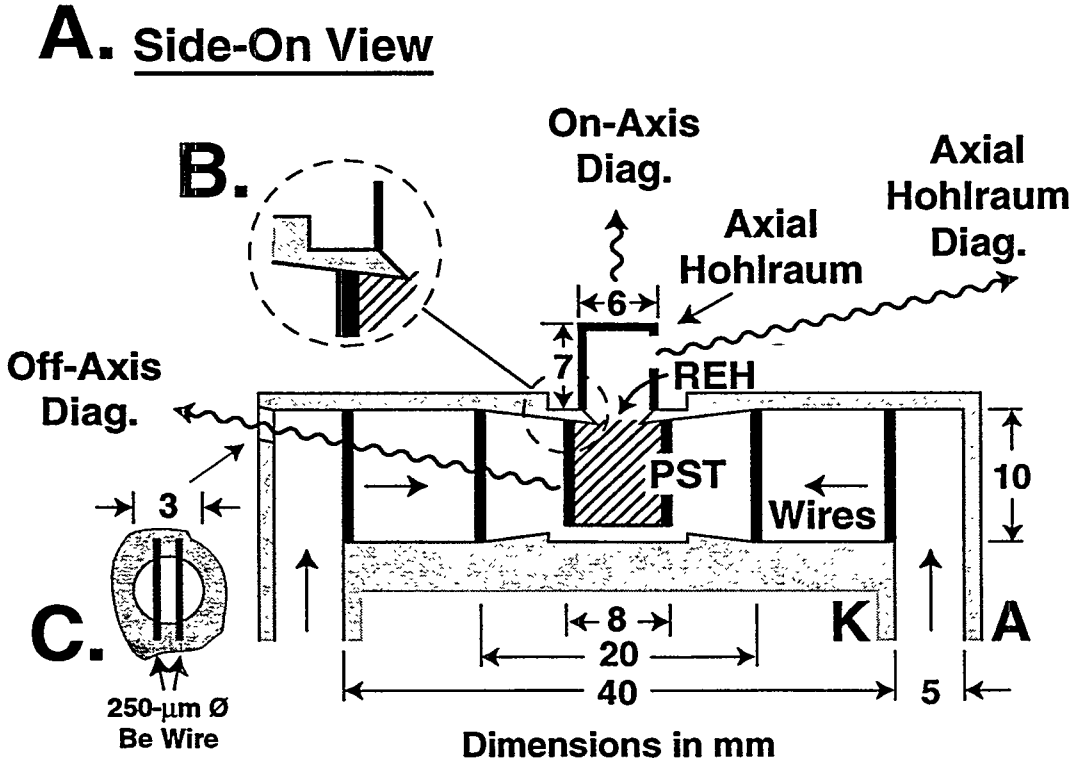

Figure 2. Schematic of single-sided, static-wall-hohlraum geometry .

EXPERIMENTAL ARRANGEMENT

Figure 2 illustrates the geometry used for the single-sided x-ray drive discussed here, and points out the location of the wire-array z-pinch load at the terminus of the Z generator, the PST, the REH, and the axial hohlraum. The use of large numbers of wires in arrays is essential for generating high radiated powers from z-pinches [9]. Nesting the arrays, moreover, enhances the power in targetless pinches [10]. Accordingly, the load in these experiments is made of outer and inner arrays of wire that number 240 and 120, respectively. In Z the load current ramps to a peak of ~20 MA in ~100 ns. The associated array diameters of 40 mm and 20 mm, array masses of 2 mg and 1 mg, and wire length of ~10 mm used and shown in *Figure 2A* are designed to approximately optimize the coupling of the generator's magnetic energy into kinetic energy of the arrays prior to stagnation. The path of the current return is through the inside of the cylindrical anode (A in *Figure 2A*)), which is solid except for a 3-mm diameter diagnostic aperture having conducting wires spaced every mm *(Figure 2C).* This design minimizes the azimuthal magnetic perturbation on the imploding array, but still permits the monitoring of the radiation generated outside the implosion. To minimize W plasma sliding across the REH and blocking the radiation generated in the central hohlraum from entering the axial hohlraum [11], the anode is slanted 3 degrees to the horizontal between the inner array and the PST *(Figure 2B).* To maintain symmetry, the cathode is similarly slanted *(Figure 2A).*

The axial hohlraums used are thin walled (25.4-μm thickness) Au cylinders, measuring either 6-mm in diameter by 7-mm in height (ignition scale [*Figure 2A*]) or 4-mm in both diameter and height. The axial-hohlraum temperature is measured with two independent diagnostics, each of which views the interior wall of the hohlraum through the same aperture (~3-mm diameter for the large hohlraum or 2-mm diameter for the small hohlraum), but at $\pm 20^{o}$ about the normal to the hole in the horizontal plane. In one diagnostic, the temperature is measured using a set of twelve silicon-diodes mounted downstream from a transmission-grating-spectrometer, which is positioned to be sensitive to x-rays in discrete energy channels spanning 100 to 600 eV. In the other diagnostic, the temperature is measured using a total-energy bolometer and a set of K- and L-edge filtered x-ray

diodes (XRDs) sensitive to x-rays in four discrete channels covering a similar energy range [6]. Plasma closure of the diagnostic hole with time is measured with a multi-filtered, fast-framing, pin-hole camera (PHC) sensitive to x-rays in four discrete spectral channels covering 100 to 600 eV [12]. Relative comparisons between the radiation detectors within each diagnostic set indicate no measurable deviation in internal azimuthal symmetry of the hohlraum with time. The peak temperature extracted from either diagnostic set agrees to within 2%±3% when averaged over the shots taken. The uncertainty refers to the RMS shot-to-shot variation. For the temperatures discussed here, a correction for the reduced hole size with time based on the averages of these images is used. The radiation entering the hohlraum is estimated by an additional suite of on-axis diagnostics [8] that view the source through the REH when the hohlraum is not present *(Figure 2A)*. These diagnostics include a total-energy bolometer, a filtered XRD set, and filtered fast-framing PHCs similar to those detectors of the horizontal diagnostic sets. Over the measured x-ray input powers P of 0.7 to 13 TW, the hohlraum temperature T scales as the Planckian relation $T\sim(P/A)^{1/4}$, where A is the surface area of the hohlraum *(Figure 3)*.

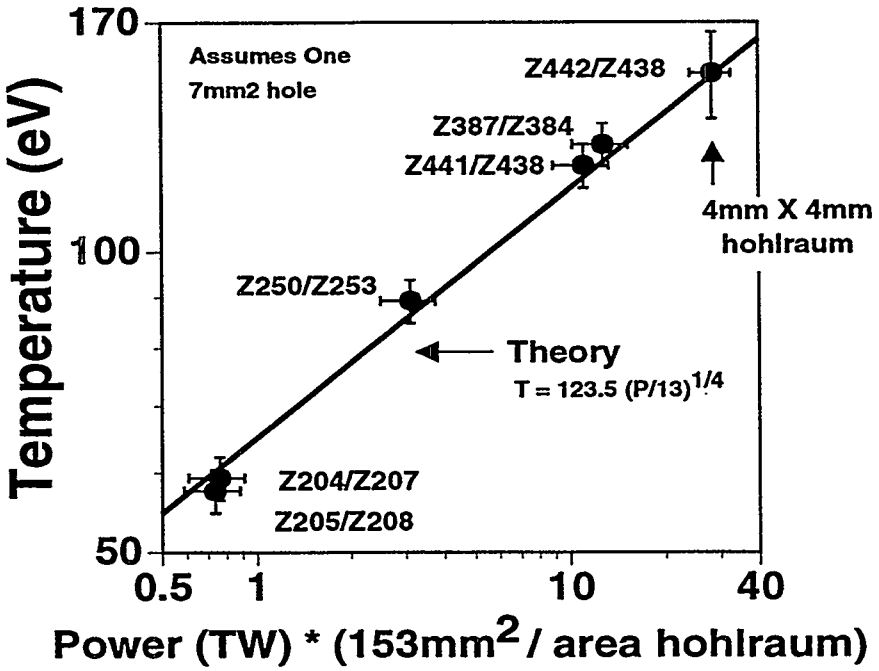

Figure 3. Measured hohlraum temperature as a function of the measured on-axis x-ray power without the hohlraum present, for the indicated shot pairs. Shown also is that expected from the $T\sim(P/A)^{1/4}$ Planckian relation, using a calculated normalization point at 13-TW [15].

In *Figure 3*, all the data except the highest temperature datum of ~150 eV correspond to those measured with the 6x7-mm^2 hohlraum.

The PSTs are constructed with a thin metal (Cu or Au) outside shell surrounding a CH-foam cylinder. The range of shell thickness, foam density, and diameter fielded includes 0-18 μg/cm^2, 0-14 mg/cm^3, and 0-8 mm, respectively. In general, increasing the diameter of the PST or mass of its components increases the duration and risetime of the x-ray pulse delivered to the hohlraum prior to final stagnation, and simultaneously decreases the initial on-axis x-ray power. For a PST of 8-mm diameter filled with 6 mg/ cm^3 foam, for example, increasing the thickness of the shell from 0 to 18 μg/cm^2 increases the pulse duration from 8 to 18 ns, the risetime from 3 to 7 ns, and reduces the peak x-ray power from 7 to 1 TW *(Figure 4)*. Radiation exterior to the PST is monitored through the small aperture *(Figure 2C)* in the current return can with a suit of off-axis diagnostics similar to that of the on-axis suite *(Figure 2A)*.

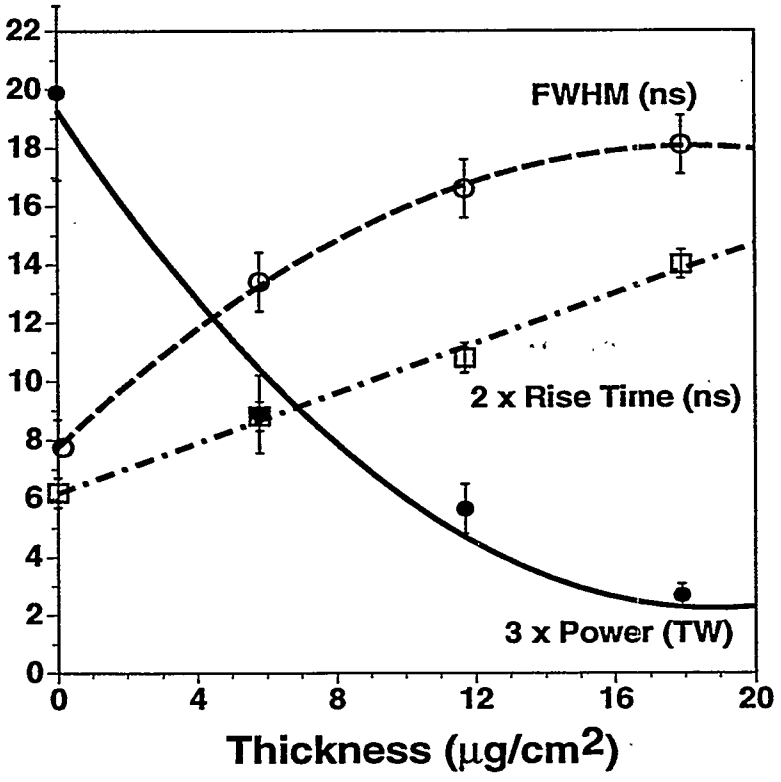

Figure 4. Peak power, risetime, and duration to final stagnation of measured on-axis x-ray pulse versus shell thickness, for a 8-mm diameter PST with 6 mg/cc foam fill.

HOHLRAUM TEMPERATURE PULSE SHAPES

Figure 1 illustrates two representative temperature pulse shapes designed to ignite 2-mm diameter Be-coated capsules on NIF. In the figure, W and D correspond to the 300-eV peak-temperature and reduced peak-temperature drive of Refs. 13 and 14, respectively. Shown also in the figure are three temperature pulse shapes measured with two different PSTs and the two different hohlraum sizes. Shots Z251 and Z441 use the 6x7-mm^2 hohlraum, while Z442 uses the 4x4-mm^2 hohlraum. Shot Z251 uses a 5.8-mm diameter REH with a PST of 8 mm diameter and a 18-$\mu g/cm^2$ Cu shell filled with 10 mg/cm^3 foam. Shots Z441 and Z442 use a 4-mm diameter REH with a 5-mm diameter PST constructed solely of 14-mg/cm^3 foam. The temperature field generated with the larger-diameter, more-massive PST matches the field required for simulating the ~85 eV, ~10-ns *foot pulse* in the NIF-scale hohlraum. The field generated with the less massive target, in contrast, provides a reasonable match for simulating the temperature associated with the *first-step pulse*. Because the solid foam target permits the pinch to compress to ~0.5-mm radial dimensions, smaller hohlraums with reduced diameters can also be efficiently heated with this target and therefore driven to yet higher temperatures. Thus, alternatively, reducing the hohlraum size with this target enables the higher temperature associated with the *next step* to be reached, as shown by the measured temperature history Z442 in *Figure 1*.

HOHLRAUM CHARACTERISTICS

Radiation-magnetohydrodynamic code (RMHC) simulations such as those of Ref. 11 are used to understand the underlying dynamics of the implosion, and to provide insight into the radiation and plasma fields inside the axial hohlraum. These simulations are 2-D integrated calculations that take into account the development of the Rayleigh-Taylor instability in the r-z plane of the imploding load, energy generation as the plasma assembles on the PST, and radiation transport (in the diffusion approximation) to the axial hohlraum.

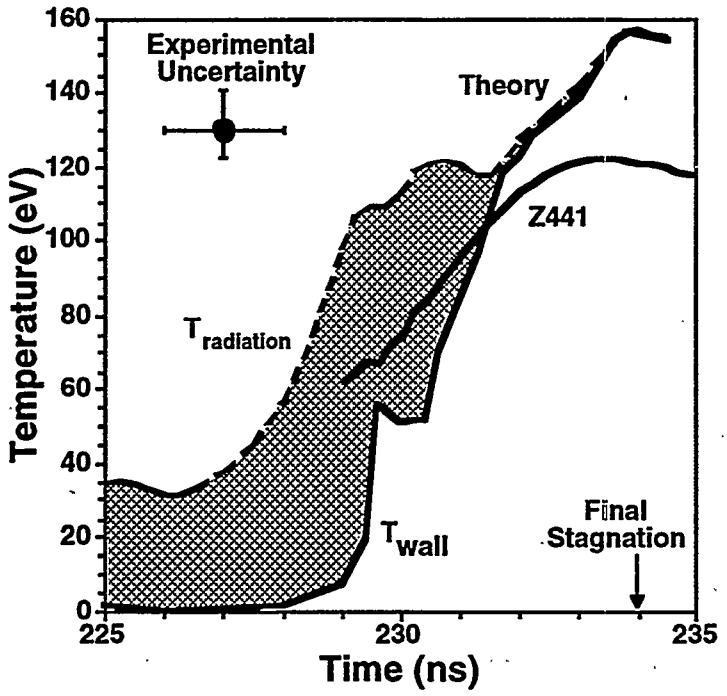

Figure 5. Comparison of the simulated radiation temperature and lower bound on the wall temperature with that measured for Shot Z441.

Figure 5 plots the simulated radiation temperature and a lower bound on the wall temperature (at an optical depth of 0.66) of the axial hohlraum 4 mm above the REH, for example, corresponding to the conditions of shot Z441. According to the simulation, the hohlraum is first bathed in a low-temperature field of ~30-40 eV (radiation pre-pulse), once the outer array strikes the inner array at ~214 ns. When the leading edge of the combined imploding plasma shell next strikes the outer edge of the PST at ~227 ns, the power entering the hohlraum rises rapidly and the associated temperature of the hohlraum quickly increases to >120 eV by ~232 ns. At this time, the plasma bubbles associated with the W shell just begin to stagnate on axis. The continued rise in the temperature between ~232 and 234 ns corresponds to the 2-D stagnation of the bubbles on axis during this final stagnation process. Maximum simulated and measured total-radiated off-axis power have been synchronized so that the peaks occur at 234 ns.

The measured temperature profiles shown in *Figure 1* all arise during the heating between the first strike on the PST and the beginning of the bubbles stagnating on axis. Experimentally, the

magnitude of the calculated temperature enhancement during final stagnation is not observed for any of the PSTs, as illustrated in the comparison shown in *Figure 5*. The absence of the enhancement in the measurements relative to the simulation may be due to: (1) 3-D effects not included in the 2-D simulation; (2) underestimates of the opacity within the compressing PST; (3) inadequacy of the diffusion approximation during pinch; (4) reduced radiation containment by the tungsten plasma during pinch; (5) underestimates of ablative closure of the REH; (6) additional W plasma sliding across the REH [11]; or possibly (7) the inadequacy of the model to predict the details of the pinch. Enabling the enhancement to occur would permit multiple-step pulses to be simulated as well as just the single steps shown in *Figure 1*. The simulations suggest, however, that even with the calculated enhancement the plasma filling the hohlraum is minimal. For the Z441 simulation of *Figure 5*, for example, between 232 and 234 ns the calculated radius of the REH has been reduced by only 0.04 to 0.2 mm, the Au wall (4 mm above the REH) has expanded radially by only 0.04 to 0.25 mm into the interior of the hohlraum, and the W plasma has expanded axially through only the ~0.5-mm depth of the REH aperture, with only CH plasma entering the axial hohlraum. *Figure 6* plots the density of this CH plasma in the axial hohlraum 2 mm above the REH, and indicates that the density remains low, about that of air, for the duration of the temperature rise.

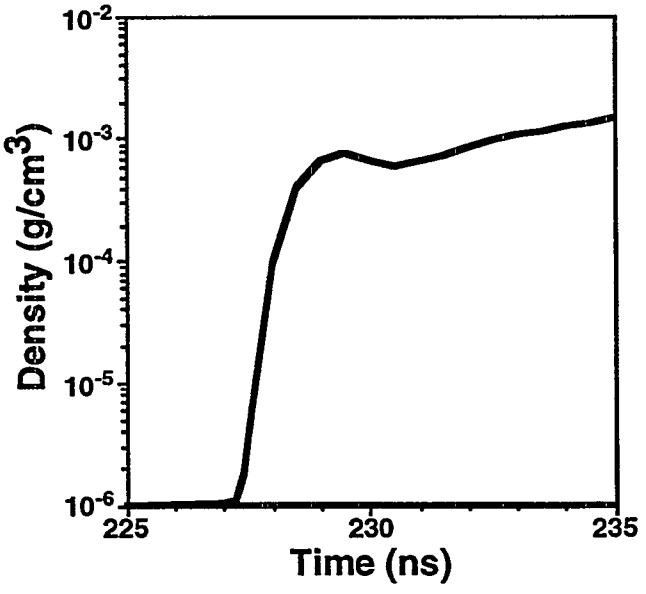

Figure 6. Simulated on-axis plasma density 2-mm above the REH for Shot Z441.

CONCLUSIONS

In conclusion, the measurements made with this single-sided-drive, static-wall-hohlraum geometry on Z have shown the ability to generate temperature pulse shapes of utility to pre-NIF studies up to peak temperatures of ~130 eV in full ignition-scale hohlraums, and ~150 eV in reduced scale hohlraums. The RMHC simulations, like the measurements [16] suggest that over useful radiation drive times, the main volume of the hohlraums remains relatively free of z-pinch plasma. Although the 2-D simulations are useful, as illustrated by *Figure 6*, a number of discrepancies remain between the characteristics calculated and measured.

If, instead of a single pinch, the wire mass were to be distributed in two independent pinches of roughly half the length of a single one (in order to maintain a similar over-all load inductance) with the axial hohlraum sandwiched between the two, the power entering the hohlraum would be roughly doubled because the on-axis power is generated primarily near the pinch ends. The peak temperature associated with this single-feed, but now two-sided x-ray drive (as in the geometry shown in *Figure 3* of Ref. 5) would then be increased to ~155 eV for the 6x7-mm^2 hohlraum [15] or ~180 eV for the 4x4-mm^2 hohlraum. Scaling this concept to a 50-MA driver, which is characteristic of the next generation z-pinch driver being considered [17], moreover, could thus provide conditions for studying implosions driven at peak temperatures in the range of 240-280 eV, depending on hohlraum size.

REFERENCES

[1] S. W. Hann, S. M. Pollaine, J. D. Lindl, et al , "Design and modeling of ignition targets for the National Ignition Facility", *Phys. Plasmas* **2**, (1995) 2480-2487.

[2] W. J. Krauser, N. M. Hoffman, D. C. Wilson, et al , "Ignition target design and robustness studies for the National Ignition Facility" *Phys. Plasmas* **3**, (1996) 2084-2093.

[3] J. D. Kilkenny, T. P. Bernat, B. A. Hammel, et al, "Lawrence Livermore National Laboratory's activities to achieve ignition by X-ray drive on the National Ignition Facility", *Laser and Part. Beams* **17**, (1999) 159-171.

[4] R. E. Olson, J. L. Porter, G. A. Chandler, *et al*, "Inertial confinement fusion ablator physics experiments on Saturn and Nova", *Phys. Plasmas* **4**, (1997) 1818-1824.

[5] R. E. Olson, G. A. Chandler, M. S. Derzon, et al., "Indirect-Drive ICF Target Concepts for the X-1 Z-Pinch Facility", *Fusion Technol.* **35**, (1999) 260-265.

[6] R. B. Spielman, C. Deeney, G. A. Chandler, et al., "Tungsten wire-array Z-pinch experiments at 200 TW and 2 MJ", *Phys. Plasmas* **5**, (1998) 2105-2111.

[7] T. W. L. Sanford, R. B. Spielman, G. O. Allshouse, *et al.*, "Wire Number Doubling in High-Wire-Number Regime Increases Z-Accelerator X-Ray Power," *IEEE Trans. Plasma Sci.* **26**, (1998) 1086-1093.

[8] T. J. Nash, M. S. Derzon, G. A. Chandler, et al, "High-temperature dynamic hohlraums on the pulse power driver Z", *Phys. Plasmas* **6**, (1999) 2023-2029.

[9] T. W. L. Sanford, R. C. Mock, R. B. Spielman, et al, "Wire array Z-pinch insights for enhanced x-ray production", *Phys. Plasmas* **6**, (1999) 2030-2040.

[10] C. Deeney, M. R. Douglas, R. B. Spielman, et al, "Enhancement of X-Ray Power from a Z Pinch Using Nested-Wire Arrays", *Phys. Rev. Lett.* **81**, (1998) 4883-4886.

[11] D. L. Peterson, R. L. Bowers, W. Matuska, et al, "Insights and applications of two-dimensional simulations to Z-pinch experiments", *Phys. Plasmas* **6**, (1999) 2178-2184.

[12] L. E. Ruggles, R. B. Spielman, J. L. Porter, and S. P. Breeze, "Characterization of a high-speed x-ray imager", *Rev. Sci. Instrum.* **66**, (1995) 712-712.

[13] D. C. Wilson, P. A. Bradley, N. M. Hoffman, et al, "The development and advantages of breyllium capsules for the National Ignition Facility", *Phys. Plasmas* **5**, (1998) 1953-1959.

[14] T. R. Dittrich, S. W. Haan, M. M. Marinak, et al, "Reduced scale National Ignition Facility capsule design", *Phys. Plasmas* **5**, (1998) 3708-3713.

[15] T. W. L. Sanford, R. E. Olson, G. A. Chandler, et al, "Z-Pinch Generated X-Rays Demonstrate Potential of Indirect Drive ICF Experiments", submitted to *Phys. Rev. Letts.* (July 1999).

[16] R. J. Leeper, T. E. Alberts, J. R. Asay, et al, "Z-Pinch Driven Inertial Confinement Fusion Target Physics Research at Sandia National Laboratories", to be published *Nuclear Fusion* (1999).

[17] K. W. Struve, et al,"ZX Pulsed-Power Design," to be published in the *Proceedings of the International Pulsed Power Conference, 1999, Monterey, CA* (June 1999).

DISTRIBUTION

3 University of New Mexico
Dept. of Chemistry & Nuclear Eng.
Attn: Prof. G. Cooper
Prof. S. Humphries
Prof. N. F. Roderick
Albuquerque, NM 87131

22 Los Alamos National Laboratory
Attn: R. J. Macek, LANSCE-D0
R. Stringfield, LANSCE-9
H. A. Thiessen, P-25
R. J. Faehl, X-1
D. L. Peterson, X-1 (3 copies)
W. Matuska,X-1 (3 copies)
R. Bowers, X-2 (3 copies)
R. Chrien, X-2
R Watt, P-22
D. Wilson, X-2
N. Hoffman, X-11
W. Krauser, X-2
E. Idzorek, P-22
W. Varnum, X-1
A. Nobile, MST-7
M. Salazar, MST-7
P. O. Box 1663
Los Alamos, NM 87545

1 Mission Research Corporation
Attn: D. R. Welch
1720 Randolph Road SE
Albuquerque, NM 87106

1 Titan Industries
Attn: R. B. Miller
P. O. Box 9254
Albuquerque, NM 87119

5 Fermilab
Attn: Prof. L. M. Lederman, Director Emeritus
J. H. Christenson
H. B. Jensen
T. E. Nash
M. Month
P. O. Box 500
Batavia, IL 60510

1 University of Michigan
Attn: Prof. Paul Drake
2455 Hayward St.
Ann Arbor, MI 48109-2143

1 University of California Davis
Attn: Prof. John deGroot
Department of Applied Science
228 Walker Hall
Davis, CA 95616

13 Naval Research Laboratory
Attn: G. Cooperstein
D. Hinshelwood
D. Mosher
J. M. Neri
P. Ottinger
F. C. Young
R. Commisso
J. Davis
K. G. Whitney
J. P. Apruzese
P. E. Pulsifer
J. L. Giuliani
W. Thornhill
4555 Overlook Ave., SW
Washington, DC 20375

1 Columbia University
Physics Department
Attn: Prof. W. Lee
538 W. 120 Street
New York, NY 10027

2 Cornell University
Laboratory of Plasma Sciences
Attn: Prof. J. B. Greenly
Prof. D. A. Hammer
369 Upson Hall
Ithaca, NY 14853-7501

2 U.S. Department of Energy
Attn: D. Crandall, DP-18
C. Keane, DP-18
19901 Germantown Rd.
Germantown, MD 20874

1 University of California at Berkeley
Nuclear Engineering
Attn: Prof. P. F. Peterson
4111 Etcheverry
Berkeley, CA 94720-1730

1 Massachusetts Institute of Technology
Plasma Fusion Center
Attn: Prof. R. D. Petrasso
167 Albany St.
Cambridge, MA 01239

1 New York University
Physics Department
Attn: Prof. J. Sculli
4 Washington Place
New York, NY 10003

1 University of Maryland
Laboratory for Plasma and Fusion Energy Studies
Attn: Prof. M. Reiser
College Park, MD 20742

4 Imperial College
Blackett Laboratory
Attn: Prof. M. G. Haines
J. P. Chittenden
F. N. Beg
S. V. Lebedev
Prince Consort Rd.
London SW7 2BZ
ENGLAND

2 Berkeley Research Associates
Attn: N. R. Pereira
J. Golden
P. O. Box 852
Springfield, VA 22150

6 Physics International Co.
Attn: H. Helava
J. Creedon
C. Gilman
Sik-Lam Wong
J. C. Riordan
P. Sincerny
2700 Merced Street
San Leandro, CA 94577

1 University of Rochester
Laboratory for Laser Energetics
Attn: J. Soures
250 East River Rd.
Rochester, NY 14623

1 General Atomics
Attn: K. Schultz
P.O. Box 85608
San Diego, CA 92186

4 Pulse Science Inc.
Attn: V. Bailey
I. Smith
J. Fockler
P. Spence
600 McCormick St.
San Leandro, CA 94577

21 Lawrence Livermore National Laboratory
Attn: P. T.Springer, L-043
A. Toor, L-041
M. D. Rosen, L-039
M. Tabak, L-015
J. H. Hammer, L-018
G. B. Zimmerman, L-030
R. S. Thoe, L-043
G. Collins, L-481
O. Landen, L-473
B. Hammel, L-481
T. Perry, L-023
D. Bradley, L-620
W. Hsing, L-021
D. Callahan-Miller, L-015
S. Haan, L-023
J. Lindl, L-039
R. Cauble, L-041
T. Dittrich, L-023
J. Kilkenny, L-488
T. Bernat, L-481
A. Wootton, L-488
P. O. Box 808
Livermore, CA 94550

1 Atomic Weapons Research Establishment
Attn: P. Thompson
Aldermaston, Reading RG7 4PR
Berkshire
ENGLAND

1 Culham Laboratory
Culham Lightning Studies Unit
Attn: C. J. Hardwick
Abingdon, Oxfordshire OX14 3DB
ENGLAND

3 Rutherford Appleton Laboratory
Attn: T. G. Walker, Director of Research and Development
P. Sharp, Director of Technology
T. Broome
Chilton, Didcot
Oxon. OX11 Oqx
ENGLAND

1 University of Delaware
Bartol Research Institute
Attn: D. Cohen
Newark, DE 19716

1 Prism Computational Sciences Inc.
Attn: J. MacFarlane
16 N. Carroll St., Suite 950
Madison, WI 53703

1 Weizmann Institute
Department of Nuclear Physics
Attn: Prof. Y. Maron
Rehovot 76100 ISRAEL

3 Kernforshungszentrum Karlsruhe Gmbh.
Attn: W. Bauer
H. Bluhm
P. Hoppe
Postfach 3640, D-7500 Karlsruhe 1
FEDERAL REPUBLIC OF GERMANY

5 C. E. R. N.
CH-1211
Attn: W. Blum
G. Jarlskog
G. Lutz
W. Manner
P. Weilhammer
Geneva 23
SWITZERLAND

1 University of Wisconsin
Fusion Technology Institute
Attn: Prof. Robert R. Peterson
1500 Engineering Dr.
Madison, WI 53706

1 MS 0513 Alton Romig, 1000
1 MS 1221 Thomas Hunter, 9000
1 MS 0839 Gerold Yonas, 16000
1 MS 1106 K. Mikkelson, 15342
1 MS 1152 Larry X. Schneider, 1643
1 MS 1153 M. T. Buttram, 15330
1 MS 1153 M. Collins Clark, 15331
1 MS 1153 P. Dale Coleman, 15331
1 MS 1155 Wendland Beezhold, 15300
1 MS 1159 M. A. Hedemann, 15344
1 MS 1165 Joe Polito, 15300
1 MS 1167 Larry D. Posey, 15343
1 MS 1167 E. Fred Hartman, 15343
1 MS 1237 Juan Ramirez, 9733
1 MS 1178 Gary Rochau, 6414
1 MS 1170 G. A. Zawadzkas, 15302
1 MS 1178 Paul Raglin, 1681
1 MS 9202 William P. Ballard, 8418
1 MS 1179 David E. Beutler, 15341
1 MS 1179 Ronald P. Kensek, 15341
1 MS 1179 J. R. Lee, 15340
1 MS 1179 L. J. Lorence, 15341
1 MS 1181 Jim Asay, 1611
1 MS 1182 Doug Bloomquist, 1630
1 MS 1182 Tim J. Renk, 15335
1 MS 1182 Steven L. Shope, 15335
1 MS 1152 Mark Kiefer, 1642
1 MS 1186 Paul L. Mix, 1642
1 MS 1186 David B. Seidel, 1642
1 MS 1193 Michael Cunio, 1673
1 MS 1186 M. P. Desjarlais, 1674
1 MS 1194 Melissa R. Douglas, 1644
1 MS 1186 Thomas Haill, 1674
1 MS 1193 David Hanson, 1673
1 MS 1186 Joel S. Lash, 1674
1 MS 1186 Barry M. Marder, 1674
1 MS 1186 Tom Mehlhorn, 1674
1 MS 1186 Stephen A. Slutz, 1674
1 MS 1186 Roger Vesey, 1674
1 MS 1193 T. L. Gilliland, 1673
1 MS 1193 Michael J. Hurst, 1673
1 MS 1193 Dan Jobe, 1673
1 MS 1187 M. Keith Matzen, 1670
1 MS 1193 John McKenney, 1673
1 MS 1193 John L. Porter, 1673
1 MS 1193 Larry E. Ruggles, 1673
1 MS 1193 Johann F. Seamen, 1673
1 MS 1193 Walter W. Simpson, 1673
1 MS 1193 Richard G. Adams, 1673
1 MS 1188 Dave Bliss, 15334
1 MS 1153 Stewart Cameron, 15336
1 MS 1188 Roy Hamil, 15334
1 MS 1188 Craig Olson, 1600
1 MS 1191 Jeff Quintenz, 1600
1 MS 1193 Dean Rovang, 1615
1 MS 1193 John Maenchen, 1615
1 MS 1194 M. G. Mazarakis, 1644
1 MS 1194 Dillon McDaniel, 1640
1 MS 1193 Peter Menge, 1615
1 MS 1194 J. Frank Camacho, 1644
1 MS 1194 Chris Deeney, 1644
1 MS 1194 S. E. Rosenthal, 1644
1 MS 1194 Rick Spielman, 1644
1 MS 1194 Ken Struve, 1644
1 MS 1194 William A. Stygar, 1644
1 MS 1196 G. A. Chandler, 1677
1 MS 0839 Mark S. Derzon, 16000
1 MS 1196 David L. Fehl, 1677
1 MS 1196 Dave Hebron, 1677

1	MS 1196	Ray J. Leeper, 1677
1	MS 1196	Raymond C. Mock, 1677
1	MS 1196	Tom J. Nash, 1677
10	MS 1196	Richard E. Olson, 1677
1	MS 1196	Carlos L. Ruiz, 1677
15	MS 1196	Thomas W. L. Sanford, 1677
1	MS 1196	F. Al Schmidlapp, 1677
1	MS 1196	Jose A. Torres, 1677
1	MS 1194	John McGurn, 1644
1	MS 1194	Stephen Breeze, 1644
1	MS 1193	Paul Primm, 1673
1	MS 1193	Johann J. Seamen, 1673
1	MS 1193	Pat Ryan, 1673
1	MS 1181	Clint A. Hall, 1611
1	MS 1192	Jerry Mills, 1636
1	MS 1196	Teresa Cutler, 1677
1	MS 1196	Steve Dropinski, 1677
2	MS 0899	Technical Library, 4916
1	MS 9018	CTF, 8940-2
1	MS 0612	Review and Approval Desk, 4912 For DOE/OSTI